



RESEARCH ARTICLE

10.1002/2016GC006317

Key Points:

- New petrological and geochemical data for the 2014–2015 Holuhraun fissure eruption
- Holuhraun lavas are compositionally similar to the Bárðarbunga volcanic system
- Multilevel magma plumbing beneath Bárðarbunga fed the Holuhraun eruption

Supporting Information:

- Supporting Information S1
- Table S1
- Table S2

Correspondence to:

F. M. Deegan,
frances.deegan@geo.uu.se

Citation:

Geiger, H., T. Mattsson, F. M. Deegan, V. R. Troll, S. Burchardt, Ó. Gudmundsson, A. Tryggvason, M. Krumbholz, and C. Harris (2016), Magma plumbing for the 2014–2015 Holuhraun eruption, Iceland, *Geochem. Geophys. Geosyst.*, 17, 2953–2968, doi:10.1002/2016GC006317.

Received 23 FEB 2016

Accepted 12 JUN 2016

Accepted article online 16 JUN 2016

Published online 5 AUG 2016

Magma plumbing for the 2014–2015 Holuhraun eruption, Iceland

Harri Geiger¹, Tobias Mattsson¹, Frances M. Deegan^{1,2}, Valentin R. Troll¹, Steffi Burchardt¹, Ólafur Gudmundsson³, Ari Tryggvason³, Michael Krumbholz¹, and Chris Harris⁴

¹Department of Earth Sciences, Mineralogy, Petrology, Tectonics, Uppsala University, Uppsala, Sweden, ²Department of Geological Sciences, Stockholm University, Stockholm, Sweden, ³Department of Earth Sciences, Geophysics, Uppsala University, Uppsala, Sweden, ⁴Department of Geological Sciences, University of Cape Town, Rondebosch, South Africa

Abstract The 2014–2015 Holuhraun eruption on Iceland was located within the Askja fissure swarm but was accompanied by caldera subsidence in the Bárðarbunga central volcano 45 km to the southwest. Geophysical monitoring of the eruption identified a seismic swarm that migrated from Bárðarbunga to the Holuhraun eruption site over the course of two weeks. In order to better understand this lateral connection between Bárðarbunga and Holuhraun, we present mineral textures and compositions, mineral-melt-equilibrium calculations, whole rock and trace element data, and oxygen isotope ratios for selected Holuhraun samples. The Holuhraun lavas are compositionally similar to recorded historical eruptions from the Bárðarbunga volcanic system but are distinct from the historical eruption products of the nearby Askja system. Thermobarometry calculations indicate a polybaric magma plumbing system for the Holuhraun eruption, wherein clinopyroxene and plagioclase crystallized at average depths of ~17 km and ~5 km, respectively. Crystal resorption textures and oxygen isotope variations imply that this multilevel plumbing system facilitated magma mixing and assimilation of low- $\delta^{18}\text{O}$ Icelandic crust prior to eruption. In conjunction with the existing geophysical evidence for lateral migration, our results support a model of initial vertical magma ascent within the Bárðarbunga plumbing system followed by lateral transport of aggregated magma batches within the upper crust to the Holuhraun eruption site.

1. Introduction

The recent Holuhraun eruption on Iceland, sometimes also referred to as Flæðahraun or Nornahraun, was a vivid reminder of the dynamic nature of magmatism in active rift settings. For Icelandic rift zones, two contrasting models of magma plumbing are usually considered. One model involves vertical magma supply from deep-seated magma reservoirs, whereas the other involves additional shallow-level lateral magma transport within the upper crust to the eventual eruption site [e.g., *Sigurdsson and Sparks, 1978; Paquet et al., 2007; Burchardt and Gudmundsson, 2009; Hartley and Thordarson, 2013*]. Lavas erupted on Iceland during rifting episodes frequently display petrological evidence for lateral transport from a central volcano [*Sigurdsson and Sparks, 1978; Eriksson et al., 2015*]. However, fissure eruptions also occur in areas lacking central volcanoes (e.g., on the Reykjanes Peninsula) and are therefore generally considered to derive through vertical magma ascent from a deep-seated mantle source [e.g., *Sigmarsson et al., 1991*].

In the case of the 2014–2015 Holuhraun eruption, seismicity and ground deformation indicated a connection between the Holuhraun eruption site and the neighboring Bárðarbunga central volcano (Figure 1) [*Riel et al., 2015; Sigmundsson et al., 2015*], which would imply that the fissure eruption was laterally fed from a reservoir beneath Bárðarbunga. In this paper, we aim to further assess the nature of this lateral connection through a first-order mineralogical and geochemical investigation. We integrate our results with the existing geological and geophysical data and examine the relative roles of vertical versus lateral magma transport prior to and during the 2014–2015 Holuhraun eruption.

1.1. Eruption Timeline

The Icelandic Meteorological Office (IMO) had documented increased volcanic unrest at Bárðarbunga in recent years [*Bjarnason, 2015*], and on the 16 August 2014, a further increase in seismic activity beneath the Bárðarbunga caldera was reported. This unrest was interpreted as reflecting ongoing magma movement

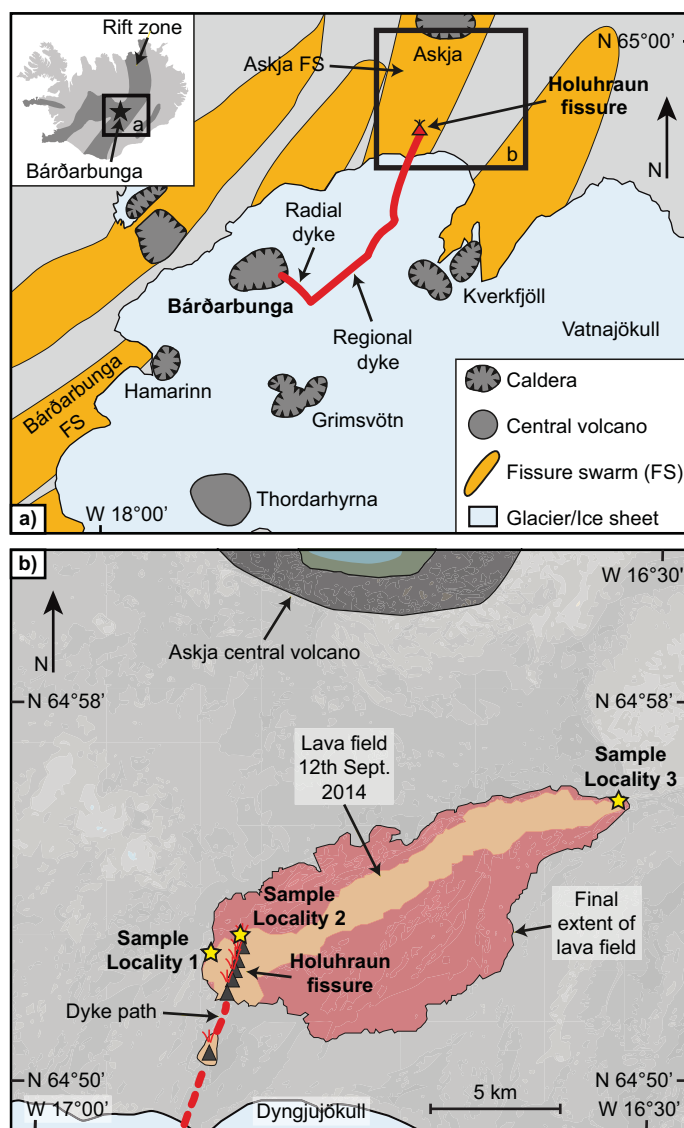


Figure 1. (a) Map of southeast Iceland showing central volcanoes and associated fissure swarms [modified after Gudmundsson and Högnadóttir, 2007]. The Holuhraun eruption site lies within the Askja fissure swarm, but seismicity prior to the eruption traced a propagating dyke from Bárðarbunga volcano. The seismic trace was first radial from the Bárðarbunga caldera margin, but soon changed direction to align with the regional fissure trends. Dyke propagation was accompanied by caldera subsidence in the Bárðarbunga caldera. (b) Map of eruption vents (dark triangles), sampling locations (yellow stars) and the extent of the Holuhraun lava field on the sampling date (12 September 2014; cream colored area), as well as the final extent of the Holuhraun lava field after the eruption ceased on the 27 February 2015 (~ 85 km², red area) [after Gíslason et al., 2015].

ued until two weeks before the eruption ended. This observation supports the existence of a lateral connection between the Bárðarbunga central volcano and the Holuhraun eruption site during the 2014–2015 eruptive events [cf. Riel et al., 2015].

2. Methods

2.1. Sampling

Lava samples were collected on 20 September 2014 from the flow front at three sites. Sample set 1 was collected at 16.8574°W, 64.8772°N and sample set 2 at 16.8333°W, 64.8833°N (Figure 1b). These two sets of

beneath Bárðarbunga. On that same day, lateral propagation of seismicity commenced, which suggested that a dyke was injected radially away from beneath the southeast edge of Bárðarbunga [Riel et al., 2015; Sigmundsson et al., 2015; Hjartardóttir et al., 2016]. After ~ 8 km, the seismic activity underwent a significant change, indicating dyke propagation toward the northeast. Approximately two weeks after this change in propagation direction, on the 29 August 2014, seismicity reached the Holuhraun site (~ 45 km to the northeast of Bárðarbunga) and lava outpouring commenced (Figure 1) [Sigmundsson et al., 2015]. The Holuhraun eruption began along a fissure that opened within the Askja fissure swarm in Iceland's North Volcanic Zone, and continued until the 27 February 2015 (Figure 1) [Gíslason et al., 2015; Sigmundsson et al., 2015]. The volume of erupted lava ($\sim 1.6 \pm 0.3$ km³) marks the Holuhraun event as the most voluminous fissure eruption since the Laki fires of 1783–1784 [Gíslason et al., 2015]. Intriguingly, one week before the onset of the Holuhraun eruption, the icecap on the Bárðarbunga caldera began to subside at a rate of ~ 1 m/d [Sigmundsson et al., 2015]. According to the Icelandic Meteorological Office (IMO), subsidence in the Bárðarbunga caldera was ongoing throughout the Holuhraun eruption and contin-

lava samples were erupted between the 2 and 3 September 2014. Sample set 3 was erupted on the 11 September 2014 and collected ~15 km to the NW from sample set 1 (at 16.5171°W, 64.9323°N; Figure 1b). Sample set 3 was collected at the furthest extent of the lava flow at that time.

2.2. Whole Rock Analyses

Whole rock sample powders were processed at Activation Laboratories Ltd., Ancaster, Canada, for major and trace element analysis. After fusion with lithium metaborate/teraborate and digestion in nitric acid, major elements were measured by inductively coupled plasma optical emission spectrometry (ICP-OES), while trace elements were analyzed by inductively coupled plasma mass spectrometry (ICP-MS). Detection limits are 0.01 wt % for all major oxides as well as for loss-on-ignition (LOI), except for MnO and TiO, which have detection limits of 0.001 wt %. See supporting information Table S1 for the full whole rock data set including detection limits. Data quality was verified by repeated analysis of internal reference materials.

2.3. Mineral Chemistry Obtained by EPMA

Mineral and groundmass compositions from 17 individual rock samples were analyzed using a Jeol JXA8530F Hyperprobe Field Emission Gun Electron Probe Microanalyser (FEG-EPMA) equipped with five spectrometers at Uppsala University. Prior to insertion into the microprobe, the sample mounts were carbon coated under vacuum. Analyses were carried out employing standard operating conditions of 15 kV accelerating voltage and 10 nA beam current. Beam diameters of 1–5 μm for mineral phases and 10 μm for groundmass were applied using counting times of 10 s on peaks and 5 s on \pm background. Groundmass analyses were carried out in grids of 5 \times 5 μm or 10 \times 10 μm , resulting in 25 or 100 data points per grid that were then averaged to produce a reliable groundmass characterization. Spectrometers 1 and 2 are equipped with TAP crystals used for the analysis of Na, Al, Si, and Mg. Spectrometer 3 is equipped with a PETJ crystal for Mn and Ti analysis. Spectrometer 4 is fitted with a PETH crystal and was used to analyze K, Ca, and Ba, while spectrometer 5 analyzed Fe, Ni, and Cr with a LIFH crystal. The instrument was calibrated with the following standards: pyrophanite for Mn and Ti, magnesium oxide for Mg, albite for Na, orthoclase for K, baryte for Ba and aluminum oxide for Al, fayalite for Fe, nickel oxide for Ni, chromium oxide for Cr, and wollastonite for Ca and Si. Analytical precision was monitored by employing the following Smithsonian Institute mineral standards: olivine (USNM 111312, $n = 490$), augite (USNM 122142, $n = 220$), Cr-augite (USNM 164905, $n = 365$), anorthite (USNM 137041, $n = 429$), Ca-plagioclase (USNM 115900, $n = 240$), and anorthoclase (USNM 133868, $n = 550$). Uncertainties are as follows: SiO_2 , Al_2O_3 , MgO and CaO $\leq 1.5\%$ s.d., FeO $\leq 2.2\%$ s.d., Na_2O in plagioclase and clinopyroxene $\leq 4.5\%$ s.d., and minor elements $\leq 10\%$ s.d. [see *Barker et al.*, 2015, for full details]. The resulting mineral data comprise 605 point analyses from 387 individual clinopyroxene crystals, 176 point analyses from 91 plagioclase crystals, and five averaged grid analyses of groundmass (see supporting information Table S2 for full mineral and groundmass compositional data set).

2.4. Mineral (-Melt) Thermobarometry

Clinopyroxene crystallization pressures and temperatures were determined using *Putirka* [2008, equations 30 and 33]. These formulations are based on the jadeite-diopside/hedenbergite exchange between clinopyroxene and an associated melt and have been shown to produce the most accurate results of all clinopyroxene thermobarometers available [*Mollo et al.*, 2010]. Both formulations require a H_2O input (see below) and the standard error of estimate (SEE) is ± 160 MPa for pressure and $\pm 45^\circ\text{C}$ for temperature.

A prerequisite for the use of mineral-melt thermobarometers is equilibrium between mineral and coexisting melt. Using the $K_{\text{D}(\text{Fe-Mg})}$ exchange coefficient, equilibrium conditions can be assumed if a clinopyroxene-melt couple falls into the $K_{\text{D}(\text{Fe-Mg})} = 0.28 \pm 0.08$ envelope [*Putirka*, 2008]. Predicted versus observed clinopyroxene components, which exploit accepted mineral exchange equilibria reactions (e.g., DiHd) [*Putirka*, 2008], are then compared. A match of the two values within ± 0.10 would validate equilibrium conditions attained from the $K_{\text{D}(\text{Fe-Mg})}$ test. We tested lava groundmass and whole rock compositions as nominal melts (see below) and used a value of 0.4 wt % H_2O in the model, based on Fourier-Transform Infrared Spectroscopy (FTIR) measurements of water contents in basaltic glasses from subglacial eruptions on Iceland [e.g., *Nichols et al.*, 2002]. This value is in line with recent measurements of water in melt inclusions in Holuhraun lavas (0.1–0.5 wt % H_2O) [*Bali et al.*, 2015] and is also indicated by the plagioclase-based hygrometer of *Putirka* [2008, equation 25b], which yields a range of H_2O contents from 0.02 to 0.38 wt % for the calculated equilibrium melts of the investigated Holuhraun plagioclase crystals.

Plagioclase-melt thermobarometry was employed on crystals and on larger microlites ($\geq 200 \mu\text{m}$), using *Putirka* [2008, equations 24a and 25a] for temperature and pressure, respectively. This model is an improved version of *Putirka* [2005], which also accounts for hydrous systems. A H_2O content of 0.4 wt % was assumed, as for the clinopyroxene thermobarometers. The SEE for this model is $\pm 247 \text{ MPa}$ for pressure and $\pm 36^\circ\text{C}$ for temperature. Similar to clinopyroxene-melt thermobarometry, accurate assessment of possible equilibrium melts is of crucial importance. In order to choose suitable plagioclase-melt pairs, the $K_{\text{D}(\text{An-Ab})}$ equilibrium test was applied to plagioclase crystals and potential melt compositions based on whole rock and groundmass data [*Putirka*, 2008] (see below). All data points that plotted within the defined envelope of $K_{\text{D}(\text{An-Ab})} = 0.10 \pm 0.05$ for $T < 1050^\circ\text{C}$ or 0.27 ± 0.11 for $T \geq 1050^\circ\text{C}$ were considered to be in equilibrium and hence appropriate for thermobarometric calculations. Mineral-melt-equilibrium thermobarometric calculations were performed using the spreadsheet provided in *Putirka* [2008].

In order to provide an independent test for the pressures obtained from equation 30, we also used a clinopyroxene-composition barometer [*Putirka*, 2008, equation 32b], which is a recalibration of the *Nimis* [1995] approach, but optimized by accounting for melt H_2O and temperature. The latter is calculated using *Putirka* [2008, equation 33] and the SEE of this model is $\pm 260 \text{ MPa}$. Additionally, we calculated pressures and temperatures of magma storage using the determined groundmass and whole rock compositions by applying the model of *Kelley and Barton* [2008], which is based on *Yang et al.* [1996] and employs the phase relations for the olivine-plagioclase-clinopyroxene cotectic boundary (OPAM). This model is independent of mineral compositions and determines P and T conditions from melt compositions alone (whole rock, groundmass) with an accuracy of $\pm 110 \text{ MPa}$ (1σ) [e.g., *Kelley and Barton*, 2008]. All single mineral and whole rock thermobarometric calculations were performed using the spreadsheets provided in *Putirka* [2008] and in *Kelley and Barton* [2008].

2.5. Oxygen Isotope Geochemistry

Oxygen isotope ratios were acquired from separated gabbroic fragments and antecryst-free whole rock lava powders using a Thermo DeltaXP mass spectrometer at the University of Cape Town, South Africa. Oxygen was extracted from approximately 10 mg of powdered sample that was dried at 50°C and subsequently degassed under vacuum at 200°C on a conventional silicate extraction line utilizing externally heated Ni vessels [*Vennemann and Smith*, 1990; *Fagereng et al.*, 2008]. Samples were then reacted with ClF_3 , and the liberated O_2 was converted to CO_2 using a hot platinized carbon rod. Unknowns were run with duplicates of the internal quartz standard (MQ) which was used to calibrate the raw data to the SMOW (Standard Mean Ocean Water) scale, using a $\delta^{18}\text{O}$ value of 10.1 for MQ (calibrated against NBS-28). All $\delta^{18}\text{O}$ results are reported in standard δ -notation, where $\delta = (R_{\text{sample}}/R_{\text{standard}} - 1) \times 1000$ and $R = {}^{18}\text{O}/{}^{16}\text{O}$. The analytical error is estimated as $\pm 0.2\text{‰}$ (2σ), based on long-term repeated analysis of MQ.

3. Results

3.1. Geochemical Classification of Minerals and Lava

All lava samples in this study are basaltic, porphyritic, and vesicular. The groundmass contains microlite plagioclase, anhedral clinopyroxene, subhedral olivine, and skeletal titanomagnetite (Figure 2). The larger crystals in the samples comprise acicular plagioclase ($\sim 6 \text{ vol } \%$, $\leq 5 \text{ mm}$), subhedral clinopyroxene ($\sim 5 \text{ vol } \%$, $\leq 2 \text{ mm}$), and subhedral olivine ($\sim 3 \text{ vol } \%$, $\leq 0.5 \text{ mm}$), which occur frequently as aggregates (glomerocrysts) (Figure 3). Plagioclase is also present in centimeter-sized, troctolite-gabbro fragments that contain minor olivine and which we hereafter refer to as gabbro fragments (Figure 4).

Olivine is either present as euhedral to subhedral microcrystals in the groundmass or as euhedral to subhedral larger crystals. Olivine also occurs as inclusions in clinopyroxene and is a constituent of the gabbro fragments (Figures 2 and 4). Olivine is zoned, occasionally resorbed, and displays a compositional range of Fo_{73-78} in cores and Fo_{66-72} in rims. Groundmass olivine is compositionally similar to the rims on the larger olivine crystals (Fo_{66-72}).

Clinopyroxene crystals are euhedral to subhedral, exhibit hourglass and complex zoning, and are commonly overgrown by thin outer rims that have a high density of olivine, titanomagnetite, and plagioclase microlite inclusions from the surrounding groundmass (Figure 2), indicating that the rims grew from the enclosing

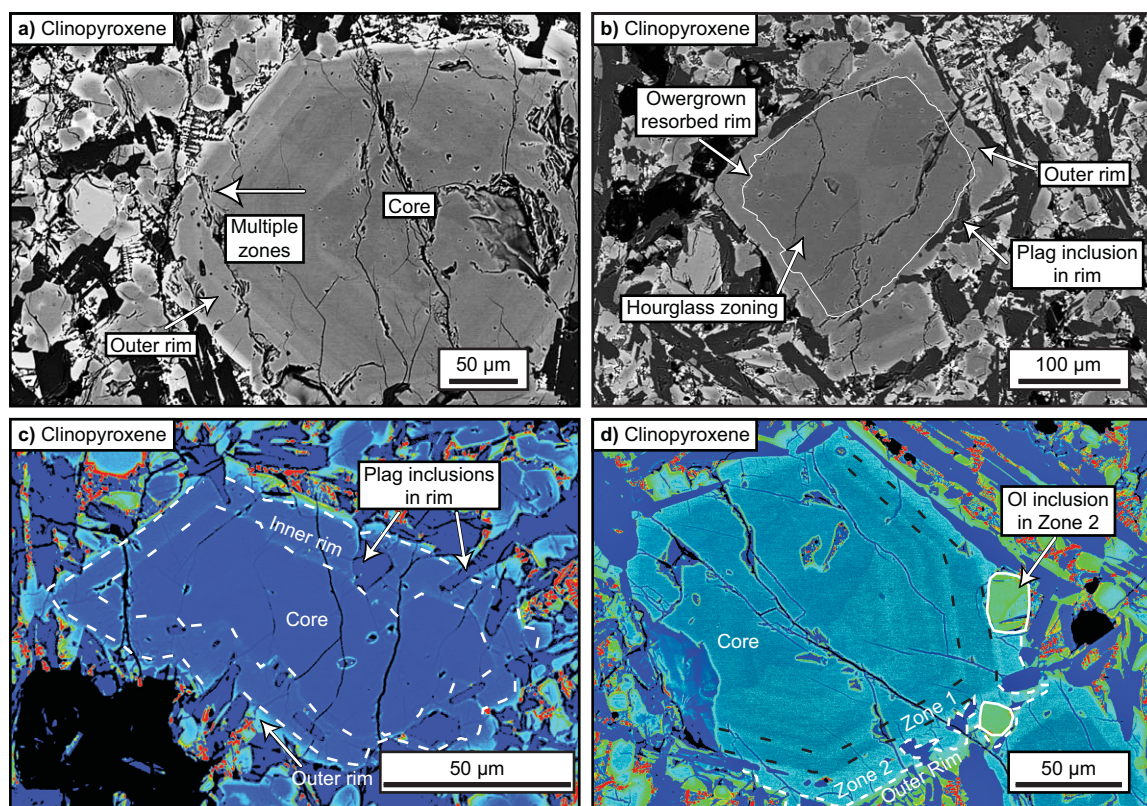


Figure 2. (a) Scanning electron microscopy (SEM) image of a clinopyroxene crystal in Holuhraun lava showing multiple internal zones. (b) SEM image of an hourglass zoned clinopyroxene, surrounded by a late grown rim that incorporated plagioclase (plag) inclusions from the surrounding groundmass. (c, d) False-color SEM images of representative clinopyroxene crystals with complex zonation. The outer rims contain frequent inclusions of groundmass crystals, confirming that the rims grew from the groundmass the crystals resided in just prior to eruption.

matrix. The compositional range of clinopyroxene extends from $Wo_{18}En_{28}Fs_9$ to $Wo_{44}En_{57}Fs_{41}$ with Mg-numbers of 43–85 (average Mg# = 77, $n = 605$) (Figure 5a).

Plagioclase crystals are euhedral to subhedral and display a compositional range of An_{54-75} with an average of An_{68} ($n = 136$). They commonly show oscillatory zonation, resorbed inner cores and embayed outer crystal rims (Figures 3a and 3b). Plagioclase in the gabbro fragments, in turn, is euhedral and has anorthite-rich cores (An_{81-90} , average An_{86} , $n = 33$) compared to its rims (An_{69-73} , average An_{72} , $n = 7$) (Figure 5b). Plagioclase also shows thin outer rims and both plagioclase and clinopyroxene show rim overgrowth superimposed on previous resorption textures (Figures 2b and 3b).

All whole rock samples fall into the basalt field of the total alkali versus silica (TAS) diagram (Figure 5c), show an average Mg-number of ~ 50 , and overlap with the field for Icelandic basalts including Askja and Bárðarbunga-Veiðivötn tephra and lavas. Groundmass analyses of the Holuhraun lavas are slightly more silica rich than the corresponding whole rock compositions and fall into the basalt and basaltic andesite fields of the TAS diagram (Figure 5c). With respect to major and trace element variations, the Holuhraun lava samples generally plot close to available compositional data from the Bárðarbunga-Veiðivötn system, but are notably different from the documented Askja sample suite (Figure 6).

3.2. Thermobarometric Modeling

Potential nominal melt compositions from this study were evaluated through the $K_{D(Fe-Mg)}$ equilibrium test for clinopyroxene-melt thermobarometry. Applying this test to clinopyroxene ($n = 605$) coupled with our new whole rock and groundmass compositions resulted in 88% of all whole rock-clinopyroxene couples and 57% of groundmass-clinopyroxene couples to fall within the $K_{D(Fe-Mg)} = 0.28 \pm 0.08$ equilibrium envelope (Figure 7). Averaged whole rock composition was therefore selected as the most suitable melt on the

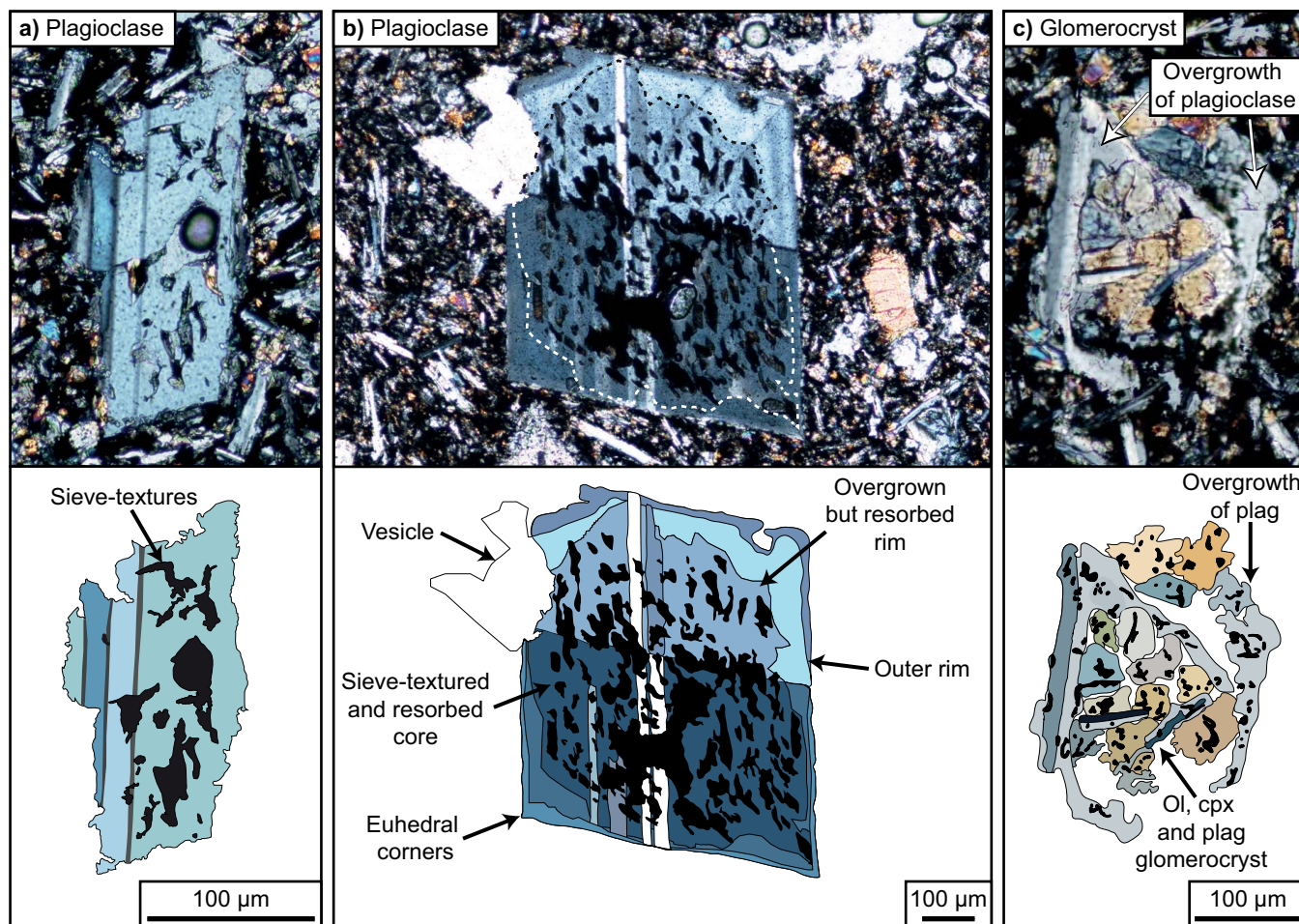


Figure 3. Microphotographs (cross-polarized light, CPL) and sketches of plagioclase in Holuhraun lava. (a) Intensely resorbed plagioclase in Holuhraun lava. (b) Well-developed (euhedral) plagioclase crystal with resorbed and sieve-textured core, but clear and continuous overgrowth rims. (c) Gabbro-type glomerocryst of olivine, clinopyroxene, and plagioclase that is overgrown by younger plagioclase rims.

basis of highest number of mineral-melt couples in equilibrium. Melt inclusions were not considered as nominal melts due to their potentially ambiguous representation of melt composition [Baker, 2008], as for example slow-diffusing elements have been shown in experimental studies to be inadequately overrepresented in melt inclusions [Baker, 2008; Neave *et al.*, 2015]. Furthermore, although a particular crystal may be in equilibrium with its own melt inclusions, the crystal may still not be directly related to the lava it erupted in or even the volcano it erupted from (i.e., it could be an ante- or a xeno-cryst).

Further refinement of the chosen equilibrium couples was performed by comparing the predicted versus observed clinopyroxene components (CaTs, EnFs, and DiHd). This exercise yielded 497 data points that fall close to the one to one line ($\pm 10\%$, Figure 7; DiHd). Data points passing these two equilibrium tests were then employed in the thermobarometric modeling.

Applying clinopyroxene-melt equilibrium thermobarometry to mineral-whole rock couples after Putirka [2008] resulted in an average crystallization pressure of 471 MPa (SEE = ± 160 MPa; model results range from 26 to 882 MPa). Assuming crustal density of 2700 kg m^{-3} , this pressure result corresponds to a crystallization depth of ~ 17 km (Figure 7) and to a calculated average temperature of 1193°C ($\pm 45^\circ\text{C}$; model results range from 1152 to 1238°C). Using the same input data, clinopyroxene-composition barometry after Nimis [1995] and Putirka [2008] produced a mean crystallization pressure of ~ 477 MPa (SEE = ± 260 MPa; model results range from 111 to 794 MPa), equivalent to ~ 18 km depth. Crystallization pressures therefore show a broad overlap between the two methods (Figure 7).

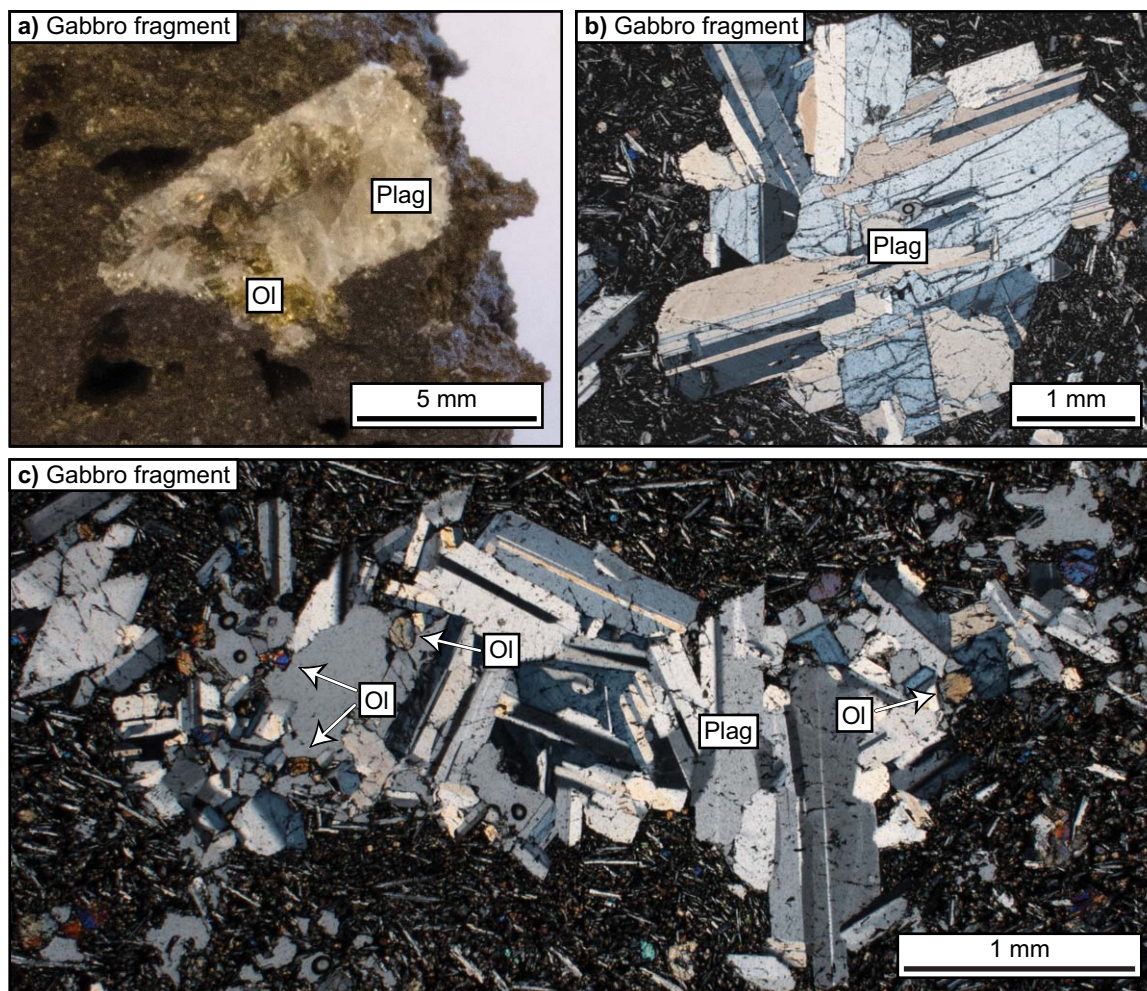


Figure 4. (a) Photograph of a typical gabbro fragment in Holuhraun lava. (b) Microphotograph of a small gabbro fragment (CPL). (c) Microphotograph of an elongated gabbro fragment in Holuhraun lava (CPL). All gabbro clasts show interlocking plagioclase and olivine crystals, and often record disintegration during transport and eruption (e.g., at the distal ends of the fragment in Figure 4c).

In contrast to clinopyroxene, very few plagioclase crystals were found to be in equilibrium with the whole rock composition, whereas groundmass compositions from the 2014–2015 Holuhraun lavas resulted in 122 out of 153 data points that satisfy equilibrium conditions for the $K_{D(\text{An-Ab})}$ equilibrium test. Plagioclase-melt thermobarometry applied to mineral-groundmass couples resulted in an average crystallization pressure of ~ 141 MPa ($\text{SEE} = \pm 247$ MPa; model results range from 103 to 165 MPa), which translates to ~ 5.2 km depth. The average crystallization depth of plagioclase is thus considerably shallower than the average pyroxene crystallization depth at ~ 17 – 18 km (Figure 7). Our mineral-melt and mineral composition based thermobarometry results are further supported by groundmass and whole rock OPAM calculations, which indicate pressures of ~ 266 MPa (9.9 km depth) for groundmass compositions and ~ 124 MPa (4.6 km depth) for whole rock (1σ uncertainty of ± 110 MPa). The thermobarometry results presented here thus indicate bimodal magma storage recorded in the Holuhraun mineral assemblage.

3.3. Oxygen Isotopes

Oxygen isotope ratios are reported in standard delta notation for five whole rock lava samples (hand-picked to exclude gabbro fragments) and five gabbro fragments (hand-picked to exclude encasing lava) (Table 1 and Figure 8). Lavas from the Holuhraun eruption show $\delta^{18}\text{O}$ values between 4.4 and 5.4‰ (avg. = 5.0‰). The gabbro fragments yield a $\delta^{18}\text{O}$ range of 4.0–5.0‰ (avg. = 4.5‰), and thus record a slightly lower range of values than the lava whole rock samples.

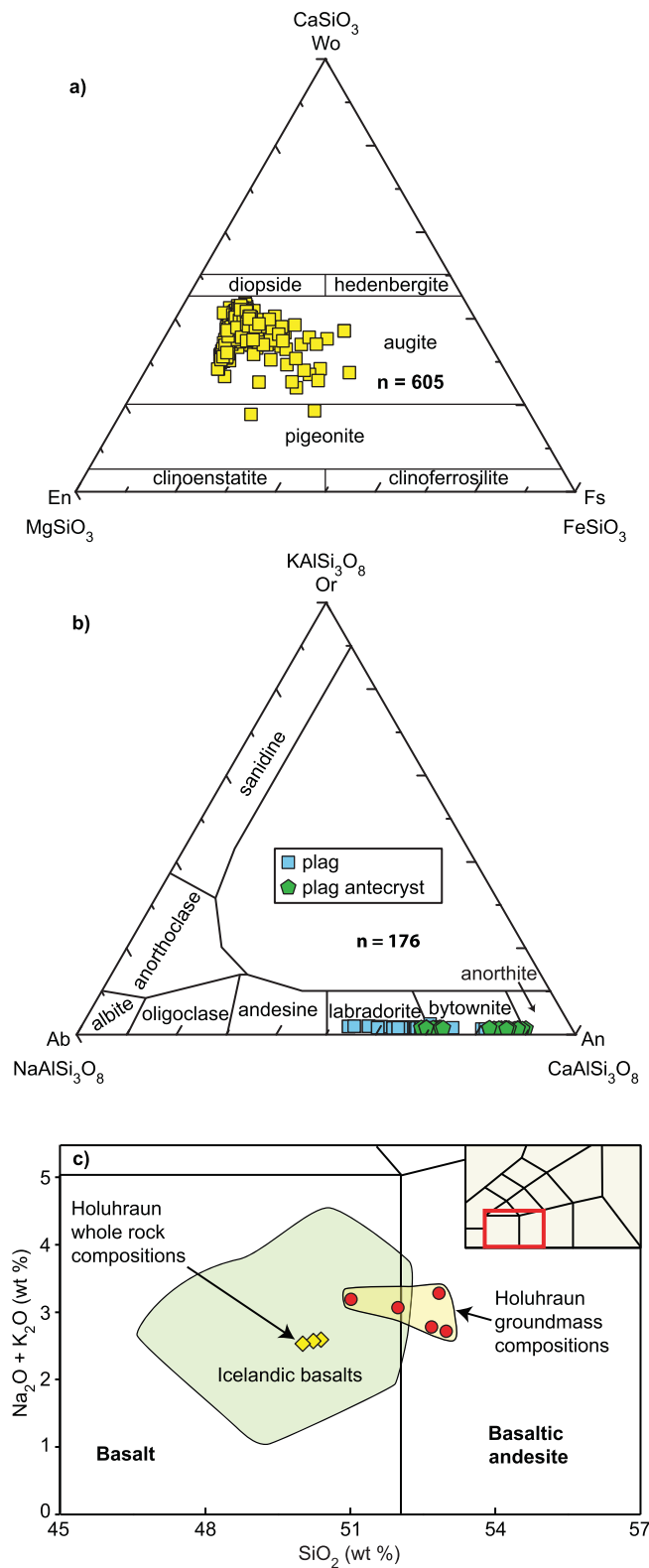


Figure 5. (a) Classification of analyzed clinopyroxene ($n = 605$) from the Holuhraun lavas following the scheme of *Morimoto et al.* [1988]. Clinopyroxene are mostly augitic. (b) Classification of plagioclase in Holuhraun lavas ($n = 176$). Plagioclase is mainly composed of bytownite and labradorite, with only minor anorthite present. (c) Total alkali versus silica (TAS) diagram showing compositions of the Holuhraun lava whole rock (yellow) and groundmass (red) from this study. The field of Icelandic basalts is shown in light green [*Hemond et al.*, 1993]. Inset shows full-scale TAS plot and the red box indicates the zoomed in area.

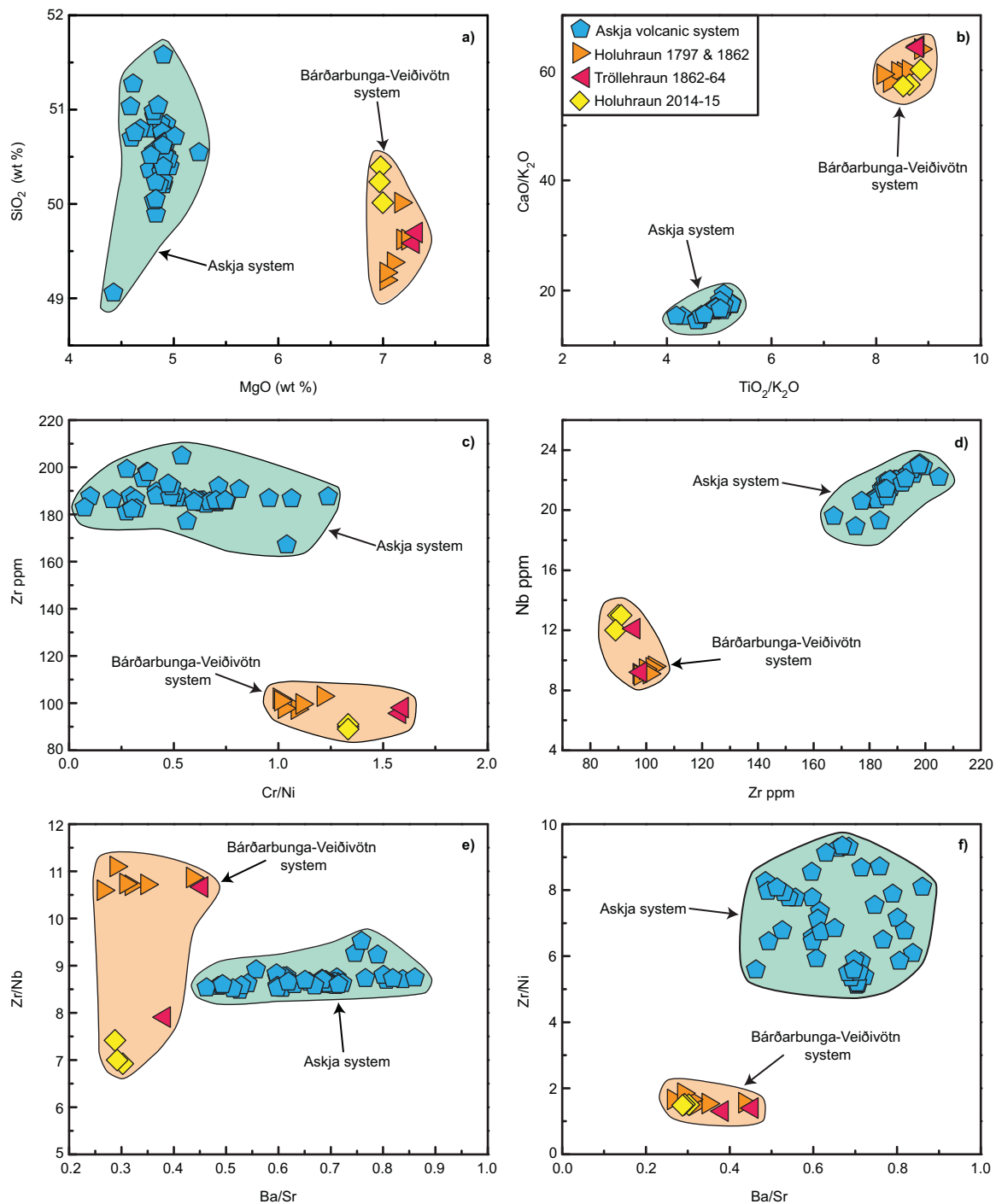


Figure 6. (a–f) Major and trace element variation diagrams of historical basaltic eruptions from the Askja and Bárðarbunga-Veiðivötn volcanic systems [Hartley and Thordarson, 2013; this study]. The Holuhraun 2014–2015 lavas consistently plot close to older eruptive products from the Bárðarbunga-Veiðivötn system, and are distinct from historical Askja products.

4. Discussion

4.1. Linking Holuhraun to Bárðarbunga

To test if the Holuhraun lavas can be linked to the Bárðarbunga volcanic system, as opposed to e.g., the nearby Askja volcano and its fissure swarm, we plotted selected major and trace element ratios in Figures 6a–6f [cf. Hartley and Thordarson, 2013]. The recent Holuhraun lavas plot close to the previous Bárðarbunga-Veiðivötn eruptive products and show higher MgO contents (~7.1 wt %) than historical Askja lavas (~4.9 wt

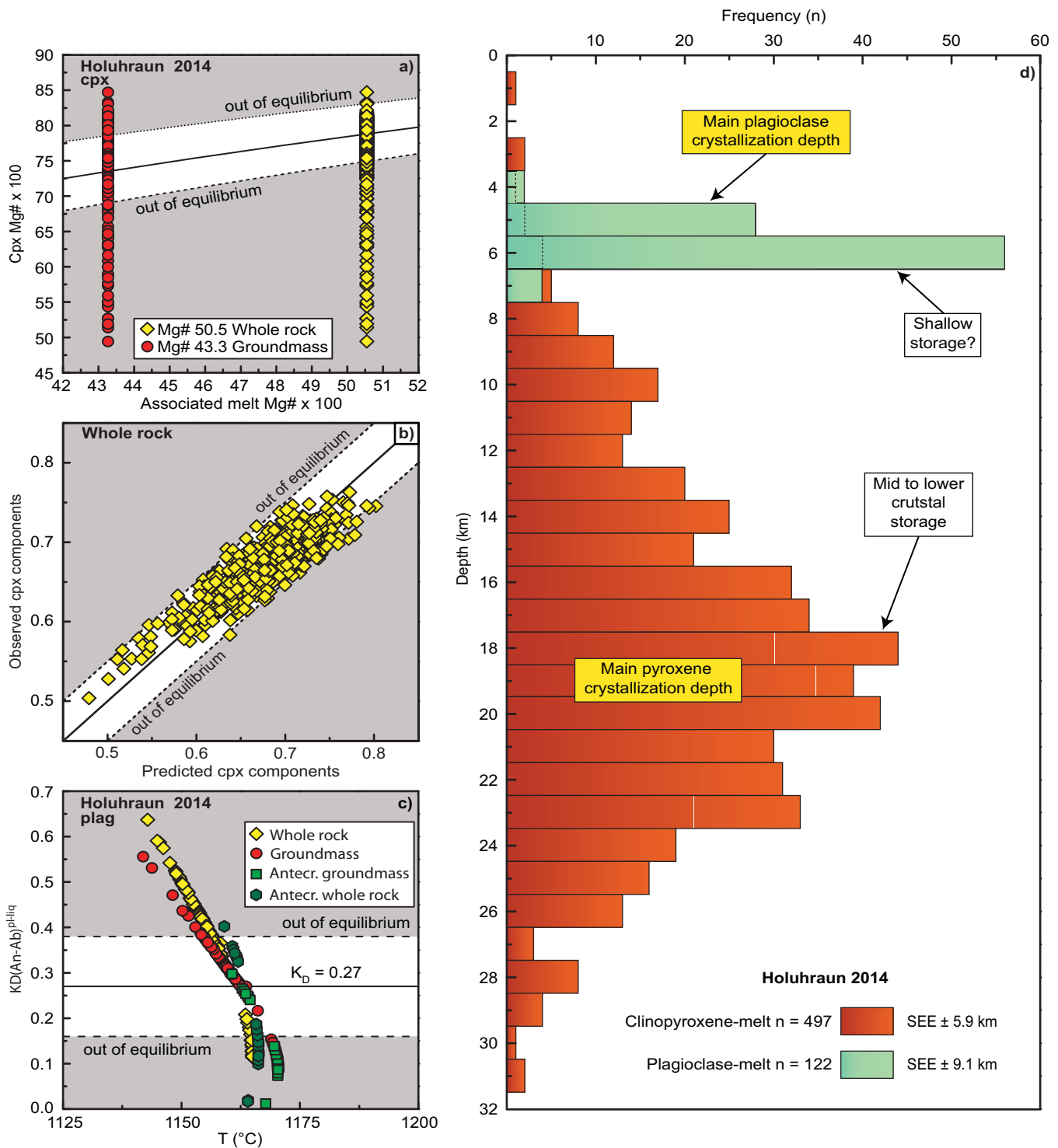


Figure 7. (a) Plot of the $K_{D(Fe-Mg)}$ equilibrium test after Putirka [2008] applied to clinopyroxene from the 2014–2015 Holuhraun eruption coupled with whole rock and groundmass compositions as possible associated melts. (b) Plot of the predicted versus observed clinopyroxene component (diopside-hedenbergite; DiHd) equilibrium test for whole rock, showing good fit as associated melt. (c) Plot of the $K_{D(An-Ab)}$ equilibrium test after Putirka [2008] applied to plagioclase from the 2014–2015 Holuhraun eruption coupled with whole rock and groundmass compositions as possible associated melts. (d) Results from clinopyroxene-melt barometry for sample sites 1–3 show an average crystallization depth of 17 km and plagioclase-melt barometry shows ~5.2 km as average depth, implying that magma from several magma storage reservoirs likely contributed to the assembly of the Holuhraun lavas.

%). Based on TiO_2/K_2O ratios, two distinct compositional groups emerge (Figure 6b), with samples from Askja plotting at TiO_2/K_2O ratios of around 5.0, while Bárðarbunga-Veiðivötn and the recent Holuhraun lavas cluster at ratios of ~8.6. In addition, CaO/K_2O ratios in Bárðarbunga-Veiðivötn and recent Holuhraun

Table 1. Oxygen Isotope Data for 2014–2015 Holuhraun Lavas and Gabbro Fragments

Sample Reference	Sample Description	Location	$\delta^{18}\text{O}$ (‰)	\pm ‰ (2 σ)
BB-1-L2	Basalt lava	16.8574°W 64.8772°N	4.4	0.2
BB-2-L1	Basalt lava	16.8333°W 64.8833°N	5.1	0.2
BB-2b-L5	Basalt lava	16.8333°W 64.8833°N	5.4	0.2
BB-3-L3	Basalt lava	16.5171°W 64.9323°N	5.1	0.2
BB-3-L4	Basalt lava	16.5171°W 64.9323°N	4.8	0.2
BB-2-X2	Troctolite ^a gabbro	16.8333°W 64.8833°N	4.9	0.2
BB-2-X5	Troctolite ^a gabbro	16.8333°W 64.8833°N	5.0	0.2
BB-3-X1	Troctolite ^a gabbro	16.5171°W 64.9323°N	4.0	0.2
BB-3-X3	Troctolite ^a gabbro	16.5171°W 64.9323°N	4.4	0.2
BB-3-X4	Troctolite ^a gabbro	16.5171°W 64.9323°N	4.4	0.2

^aReferred to as gabbro fragments in main text.

samples exceed the respective ratios in the Askja lavas by a factor of three. Ratios of the compatible trace elements Cr/Ni range between 1.0 and 1.6 for Bárðarbunga-Veiðivötn and recent Holuhraun lavas, while the range for Askja lavas is lower at ~0.4–1.2. Similarly, Ba/Sr ratios in Askja lavas are distinct from Bárðarbunga-Veiðivötn/Holuhraun lavas (~0.66 versus ~0.33, respectively) as are the concentrations of incompatible elements Zr and Nb (~100 ppm versus ~10 ppm and ~190 ppm versus ~20 ppm, respectively). On the basis of major and trace element geochemistry, a compositional affinity between the 2014–2015 Holuhraun lavas and the Bárðarbunga-Veiðivötn system is therefore apparent. This result corroborates the geophysical data that point to a lateral connection between Bárðarbunga volcano and the 2014–2015 Holuhraun fissure eruption [Riel et al., 2015; Sigmundsson et al., 2015].

4.2. Origin of the Gabbro Fragments

Gabbro fragments in the 2014–2015 Holuhraun lavas have textures characteristic of crystal mushes that accumulate at magma reservoir walls and margins (Figure 4) [cf. Marsh, 2013]. Gabbroic bodies are typical at shallow to midcrustal levels beneath central volcanoes in the North Atlantic Igneous Province [e.g., Emeleus and Bell, 2005; Gurenko and Sobolev, 2006; Paquet et al., 2007; O’Driscoll et al., 2008; Burchardt and Gudmundsson, 2009]. Plagioclase in the Holuhraun gabbro fragments have crystal cores that are more calcic than the plagioclase in the lavas, but their crystallization depth could not be estimated because they did

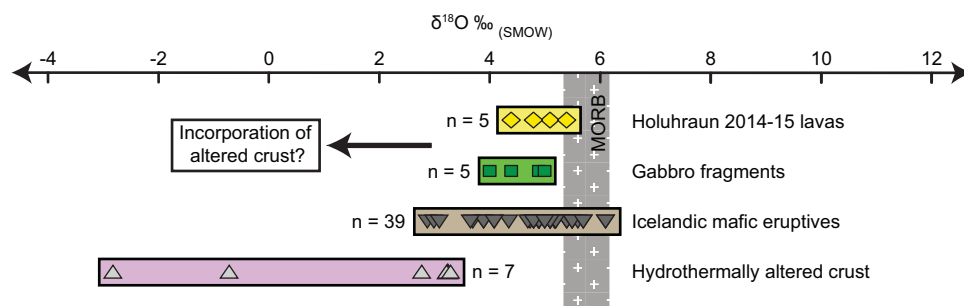


Figure 8. Plot showing $\delta^{18}\text{O}$ values for the Holuhraun lavas and the gabbroic fragments compared to Mid-Ocean Ridge Basalt (MORB) [Bindeman et al., 2008], Icelandic mafic eruptive products [Sigmarsson et al., 1991; Gunnarsson et al., 1998; Hards et al., 2000; Prestvik et al., 2001; Bindeman et al., 2008], and altered crustal rocks [Prestvik et al., 2001; Bindeman et al., 2006, 2008]. Note that the $\delta^{18}\text{O}$ values of the gabbro fragments are displaced to below MORB values, while the lava samples extend from the MORB range toward values characteristic of the gabbro fragments, implying that assimilation of gabbro fragments likely caused the shift toward sub-MORB values in the lava samples.

not equilibrate with whole rock or groundmass compositions of the 2014–2015 Holuhraun lavas (Figure 7). On the other hand, the rims of gabbro-derived plagioclase are in equilibrium with the groundmass compositions and record relatively shallow crystallization pressures (Figure 7).

Furthermore, the gabbro fragments show a slightly lower $\delta^{18}\text{O}$ range than the lavas (Table 1 and Figure 8), implying that they might be of a different origin [cf. Bindeman *et al.*, 2006; Neave *et al.*, 2013]. Oxygen isotope ratios lower than Mid-Ocean Ridge Basalt (MORB) can result from the incorporation of ^{18}O -depleted crust by the gabbroic crystal mushes during solidification [Bindeman *et al.*, 2006, 2008], from hydrothermal overprinting [e.g., Forester and Taylor, 1976; Norton and Taylor, 1979; Fridleifsson, 1983], or from a primary mantle-derived low- $\delta^{18}\text{O}$ magma [e.g., Macpherson *et al.*, 2005; Winpenny and MacLennan, 2014]. In this respect, widespread resorption textures in the gabbro fragments (see Figures 3a and 3b) indicate a lower melting point relative to the intruding magma, which could be caused by higher water content in the gabbro [cf. Yoder and Tilley, 1962]. The gabbro fragments would potentially gain water if they were hydrated after their initial solidification by hydrothermal overprinting or, alternatively, by assimilation of relatively hydrated hydrothermally altered crustal rock during solidification [cf. Humphris and Thompson, 1978]. The presence of entrained gabbro fragments in the Holuhraun lavas (Figure 4) [cf. Gurenko and Sobolev, 2006; Paquet *et al.*, 2007], their shallow crystallized plagioclase rims that overgrew resorption textures, and their relatively low- $\delta^{18}\text{O}$ values imply that at least part of the Holuhraun magma was sourced from a complex plumbing system beneath a central volcano. Assimilation of high-level and low- $\delta^{18}\text{O}$ crystal mushes and/or partially crystallized chamber walls or intrusions by ascending basalt magma could then also explain the observed spread in the $\delta^{18}\text{O}$ values of gabbro-free Holuhraun lava, which range from MORB values to those typical of the gabbro fragments [cf. Bindeman *et al.*, 2006, 2008].

4.3. Magmatic Processes Prior to the Holuhraun Eruption

With respect to preeruptive magmatic processes, we note that approximately 60% of the crystals investigated show textural evidence for resorption and multistage growth, which is most probably a function of crystal entrainment in melt(s) of differing composition and thermal properties and was likely aided by pressure release during multistage transport to the surface (Figures 3a and 3b) [cf. Browne *et al.*, 2006; Mollo *et al.*, 2010; Gurenko and Sobolev, 2006]. In addition, mixed crystal populations were identified, comprising different size and compositional groups, which emphasizes that the Holuhraun lavas represent an assembly of magma batches that originally crystallized at different depths (Figures 2–4). Breakdown textures in the gabbro fragments and overgrown resorption textures in plagioclase and clinopyroxene further support multistage magma ascent (Figures 2 and 3). Moreover, these observations are consistent with our thermobarometric calculations that identified polybaric magma storage (see section 3.2 and below). Therefore, the lavas erupted at Holuhraun were evidently supplied by a multitiered plumbing system as opposed to having been directly derived from greater depth prior to eruption.

In detail, clinopyroxene barometry reveals an average storage level at ~ 17 – 18 km depth beneath the surface. There is large spread in the distribution of estimated clinopyroxene crystallization pressures ($SEE = 160$ MPa) [Putirka, 2008] and the distribution is slightly skewed to lower pressures (Figure 7d). The distribution of estimated plagioclase crystallization, in turn, is narrowly focused at between 5 and 6 km ($SEE = 247$ MPa) [Putirka, 2008]. The thermobarometry calculations thus provide evidence for dominant pyroxene crystallization at midcrustal levels, while the plagioclase crystals appear to have grown dominantly at shallow crustal levels. These results are consistent with magma mixing during ascent beneath Bárðarbunga and would also explain the oxygen isotope data in terms of magma-crust interaction involving Icelandic upper crust (Figure 7) [cf. Sigmarsson *et al.*, 2011]. We note here, however, that the clinopyroxene mineral-melt thermobarometry after Putirka [2008] has recently been suspected of potentially overpredicting crystallization pressures for Icelandic magmas [Neave *et al.*, 2015]. Yet as there is no specific calibration for Icelandic magmas available and as mineral-melt thermobarometry results are in general agreement with the bimodality obtained from OPAM pressure calculations on groundmass and whole rock compositions (see section 3.2 above), we argue that the approach employed here produces the currently most viable depth estimates of crystallization for the Holuhraun system. This suggestion is further strengthened by the overlap observed between our thermobarometry results and the crystallization pressures obtained from previous eruptions connected to Bárðarbunga. For example, Kelley and Barton [2008] identified crystallization depths between 10 and 31 km below Bárðarbunga using the olivine-plagioclase-clinopyroxene cotectic after Yang *et al.* [1996], whereas Hartley and Thordarson [2013] reported depths between 9 and 28 km using clinopyroxene-melt

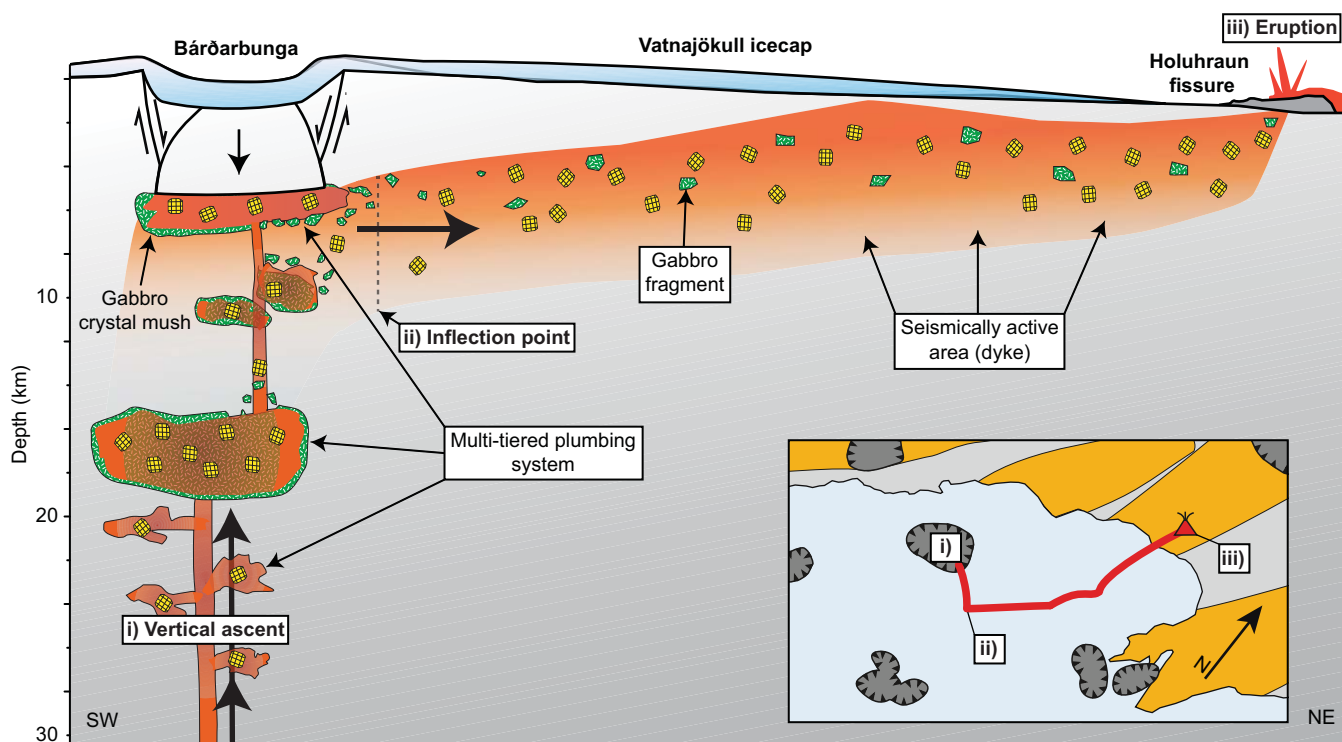


Figure 9. Conceptual model of the magma plumbing system for the 2014–2015 Holuhraun eruption. Considering our results in the context of the current geological framework [e.g., Riel *et al.*, 2015; Sigmundsson *et al.*, 2015], we envisage that (i) magma ascended from ~17 km depth to shallow crustal levels beneath Bárðarbunga in mid-August 2014 where it intersected an existing magma reservoir. (ii) Magma from distinct reservoirs was then aggregated and transported laterally for some distance to produce the final erupted Holuhraun lava (iii). The erupted lava records multiple crystal populations, entrained gabbro fragments, and ^{18}O -depleted (i.e., crustal) oxygen isotope ratios relative to MORB. The inset shows the propagation of the dyke in schematic cross section and in map view.

thermobarometry after Putirka [2008] on older Bárðarbunga-Veiðivötn eruptives. Moreover, calculations on volatile solubility in melt inclusions point to a storage depth between 3 and 12 km, and deep earthquakes at 12–25 km depths were reported in the vicinity of Bárðarbunga volcano in the years preceding the recent eruption [Hartley *et al.*, 2016]. In combination with our results, these studies therefore lend increasing support to the concept of long-term multitiered magma plumbing beneath the Bárðarbunga central volcano.

Our thermobarometry results can be further tested against results from geophysical methods [cf. Dahrén *et al.*, 2012; Martí *et al.*, 2013; Longpré *et al.*, 2014]. For instance, our clinopyroxene-melt thermobarometric results are consistent with GPS displacement modeling, which constrained the depth of a deflation source beneath Bárðarbunga to 16.8 km [Green *et al.* 2015]. The shallower crystallisation depths recorded by our plagioclase-melt thermobarometry results, in turn, are supported by earthquake hypocenters at <5 km depth in the decades prior to the Holuhraun eruption that indicated magma movement beneath Bárðarbunga volcano [Bjarnason, 2015]. Moreover, seismic evidence of radial dyke initiation also points to the existence of an overpressurized shallow magma reservoir [Grosfils, 2007; Galland *et al.*, 2014]. Lastly, we note that geodetic modeling of the deformation associated with the propagating dyke in August 2014 favors an even shallower magma source (~1–3 km) [Riel *et al.*, 2015; Sigmundsson *et al.*, 2015], which is still within the uncertainties of our plagioclase-melt thermobarometry results. Hence, and despite the model inherited errors (see section 3.2 above), our thermobarometric results are in good agreement with estimates from both geochemical and geophysical approaches.

In summary, we envisage the following sequence of events to have led to the 2014–2015 Holuhraun eruption (Figure 9): (i) Magma initially ascended vertically from ~17 km depth within the Bárðarbunga plumbing system to relatively shallow levels where it interacted with high-level magma and crystal mushes of the Bárðarbunga plumbing system. (ii) From there, a radial dyke was injected and propagated within the local, volcano-controlled stress field [cf. Sigmundsson *et al.*, 2015]. (iii) When the dyke reached beyond the influence of the local volcanic stress field, it changed direction and propagated parallel to the regional stress

field toward the Holuhraun eruption site, where it eventually broke through to the surface. In combination with available seismic and ground deformation data [Riel *et al.*, 2015; Sigmundsson *et al.*, 2015], it becomes apparent that after initial emplacement of a radial dyke, lateral, long-distance magma transport from Bárðarbunga occurred prior to eruption at Holuhraun (Figure 9), since geophysical and geochemical data identify Bárðarbunga volcano as the source of the Holuhraun lavas. Lateral magma drainage is thus the most plausible reason for the simultaneous fissure eruption at Holuhraun and caldera subsidence at Bárðarbunga.

5. Conclusions

The petrological evidence for recent Holuhraun lavas presented here implies that the lavas were derived from a complex and interconnected magma plumbing system spanning between 28 and 5 km depth beneath the Bárðarbunga central volcano wherein discrete magma batches interacted and mixed. Magma initially pooled around 17–18 km depth on average, whereafter it ascended and was temporarily stored at high crustal levels within Bárðarbunga. There, the magma interacted with, and entrained, gabbro fragments and crystal mushes that are characterized by resorption and disintegration textures and $\delta^{18}\text{O}$ values lower than MORB. The magma was then laterally transported away from the shallow parts of the Bárðarbunga plumbing system first via a radial dyke and then via a regional dyke until the magma eventually broke through to the surface at the Holuhraun eruption site. The latest Holuhraun rifting episode therefore involved lateral magma drainage and mobilization of preexisting magma batches and mushes from relatively shallow reservoirs beneath a central volcano, and appears to represent a viable trigger for caldera subsidence at Bárðarbunga. This combination of phenomena reflects a potentially underappreciated geodynamic possibility that may need to be incorporated into hazard assessment in active volcanic rift-zone settings.

Acknowledgments

We are grateful to Börje Dahrén, David A. Budd, Abigail K. Barker, Ester M. Jolis, Kristín Jónsdóttir, Morten S. Riishus, John MacLennan, and Eoghan Holohan for insightful discussions and to Giulia Sgattoni who helped with sampling. Kristín Jónsdóttir from the Icelandic Meteorological Office is also thanked for providing complementary samples, and Dan Zetterberg is thanked for producing thin sections at Stockholm University. The Icelandic Meteorological Office (IMO) is furthermore acknowledged for open access publication of information on the Holuhraun eruption (<http://en.vedur.is/earthquakes-and-volcanism/articles/nr/2947>). This work was supported by the Swedish Research Council (VR) and the Centre for Natural Disaster Science (CNDS). The data for this paper are available in the text, tables, and references therein, and in the supporting information.

References

- Baker, D. R. (2008), The fidelity of melt inclusions as records of melt composition, *Contrib. Mineral. Petrol.*, *156*, 377–395, doi:10.1007/s00410-008-0291-3.
- Bali, E., O. Sigmundsson, S. Jakobsson, and H. Gunnarsson (2015), Volatile budget of the Nornahraun eruption of the Bárðarbunga system, Iceland, in *Geophysical Research Abstracts, EGU General Assembly 2015*, vol. 17, pp. EGU2015-5757.
- Barker, A. K., V. R. Troll, J.-C. Carracedo, and P. A. Nicholls (2015), The magma plumbing system for the 1971 Tenguia eruption, La Palma, Canary Islands, *Contrib. Mineral. Petrol.*, *170*, 54, doi:10.1007/s00410-015-1207-7.
- Bindeman, I. N., O. Sigmundsson, and J. Eiler (2006), Time constraints on the origin of large volume basalts derived from O-isotope and trace element mineral zoning and U-series disequilibria in the Laki and Grímsvötn volcanic system, *Earth Planet. Sci. Lett.*, *245*, 245–259, doi:10.1016/j.epsl.2006.02.029.
- Bindeman, I. N., A. Gurenko, O. Sigmundsson, and M. Chaussidon (2008), Oxygen isotope heterogeneity and disequilibria of olivine crystals in large volume Holocene basalts from Iceland: Evidence for magmatic digestion and erosion of Pleistocene hyaloclastites, *Geochim. Cosmochim. Acta*, *72*, 4397–4420, doi:10.1016/j.gca.2008.06.010.
- Bjarnason, I. T. (2015), Earthquake sequence 1973–1996 in Bárðarbunga Volcano: Seismic activity leading up to eruptions in the NW-Vatnajökull area, *Jökull*, *64*, 61–82.
- Browne, B. L., J. C. Eichelberger, L. C. Patino, T. A. Vogel, K. Uto, and H. Hoshizumi (2006), Magma mingling as indicated by texture and Sr/Ba ratios of plagioclase phenocrysts from Unzen volcano, SW Japan, *J. Volcanol. Geotherm. Res.*, *154*, 103–116, doi:10.1016/j.jvolgeores.2005.09.022.
- Burchardt, S., and A. Gudmundsson (2009), The infrastructure of Geitafell volcano, southeast Iceland, in *Studies of Volcanology: The Legacy of George Walker, Spec. Publ. of IAVCEI*, vol. 2, edited by T. Thordarson *et al.*, pp. 349–369, Geol. Soc., London, U. K.
- Dahrén, B., V. R. Troll, U. B. Andersson, J. P. Chadwick, M. F. Gardner, K. Jaxybulatov, and I. Koulakov (2012), Magma plumbing beneath Anak Krakatau volcano, Indonesia: Evidence for multiple magma storage regions, *Contrib. Mineral. Petrol.*, *163*, 631–651, doi:10.1007/s00410-011-0690-8.
- Emeleus, C. H., and B. R. Bell (2005), *The Palaeogene Volcanic Districts of Scotland*, 4th ed., Br. Geol. Sur., 214 pp., Nottingham, U. K.
- Eriksdottir, P. I., M. S. Riishuus, and S.-Å. Elming (2015), Magma flow and palaeo-stress deduced from magnetic fabric analysis of the Álfafjörður dyke swarm: Implications for shallow crustal magma transport in Icelandic volcanic systems, in *The Use of Palaeomagnetism and Rock Magnetism to Understand Volcanic Processes*, edited by H. M. Ort, M. Porreca, and J. W. Geissman, *Geol. Soc. London, Spec. Publ.*, *396*, 107–132.
- Fagereng, Å., C. Harris, M. La Grange, and G. Stevens (2008), Stable isotope study of the Archaean rocks of the Vredefort impact structure, central Kaapvaal Craton, South Africa, *Contrib. Mineral. Petrol.*, *155*, 63–78, doi:10.1007/s00410-007-0224-6.
- Forester, R. W., and H. P. Taylor (1976), ^{18}O -depleted igneous rocks from the Tertiary complex of the Isle of Mull, Scotland, *Earth Planet. Sci. Lett.*, *32*, 11–17, doi:10.1016/0012-821X(76)90178-3.
- Fridleifsson, G. O. (1983), Geology and the alteration history of the Geitafell central volcano, southeast Iceland, PhD thesis, Univ. of Edinburgh, U. K. [Available at <http://hdl.handle.net/1842/13860>.]
- Galland, O., S. Burchardt, E. Hallot, R. Mourgues, and C. Bulois (2014), Dynamics of dikes versus cone sheets in volcanic systems, *J. Geophys. Res. Solid Earth*, *119*, 6178–6192, doi:10.1002/2014JB011059.
- Gíslason, S. R., *et al.* (2015), Environmental pressure from the 2014–15 eruption of Bárðarbunga volcano, Iceland, *Geochem. Perspect. Lett.*, *1*, 84–93, doi:10.7185/geochemlet.1509.

- Green, R. G., T. Greenfield, and R. S. White (2015), Triggered earthquakes suppressed by an evolving stress shadow from a propagating dyke, *Nat. Geosci.*, *8*, 629–632, doi:10.1038/ngeo2491.
- Grosfils, E. B. (2007), Magma reservoir failure on the terrestrial planets: Assessing the importance of gravitational loading in simple elastic models, *J. Volcanol. Geotherm. Res.*, *166*, 47–75, doi:10.1016/j.jvolgeores.2007.06.007.
- Gudmundsson, M. T., and T. Högnadóttir (2007), Volcanic systems and calderas in the Vatnajökull region, central Iceland: Constraints on crustal structure from gravity data, *J. Geodyn.*, *43*, 153–169, doi:10.1016/j.jog.2006.09.015.
- Gunnarsson, B., B. D. Marsh, and H. P. Taylor (1998), Generation of Icelandic rhyolites: Silicic lavas from the Torfajökull central volcano, *J. Volcanol. Geotherm. Res.*, *83*, 1–45, doi:10.1016/S0377-0273(98)00017-1.
- Gurenko, A. A., and A. V. Sobolev (2006), Crust–primitive magma interaction beneath neovolcanic rift zone of Iceland recorded in gabbro xenoliths from Midfell, SW Iceland, *Contrib. Mineral. Petrol.*, *151*, 495–520, doi:10.1007/s00410-006-0079-2.
- Hards, V. L., P. D. Kempton, R. N. Thompson, and P. B. Greenwood (2000), The magmatic evolution of the Snæfell volcanic centre: an example of volcanism during incipient rifting in Iceland, *J. Volcanol. Geotherm. Res.*, *99*, 97–121, doi:10.1016/S0377-0273(00)00160-8.
- Hartley, M. E., and T. Thordarson (2013), The 1874–1876 volcano-tectonic episode at Askja, North Iceland: Lateral flow revisited, *Geochem. Geophys. Geosyst.*, *14*, 2286–2309, doi:10.1002/ggge.20151.
- Hartley, M. E., E. Bali, J. Maclennan, M. Edmonds, T. Thordarson, and E. Ilyinskaya (2016), Volatile budget of the 2014–15 Nornahraun eruption, Iceland, in *VMSG Conference Abstracts 2016*, 48 pp., Trinity College Dublin, Ireland.
- Hemond, C., N. T. Arndt, U. Lichtenstein, A. W. Hofmann, N. Oskarsson, and S. Steinthorsson (1993), The heterogeneous Iceland plume: Nd–Sr–O isotopes and trace element constraints, *J. Geophys. Res.*, *98*, 15,833–15,850, doi:10.1029/93JB01093.
- Hjartardóttir, A. R., P. Einarsson, M. T. Gudmundsson, and T. Högnadóttir (2016), Fracture movements and graben subsidence during the 2014 Bárðarbunga dike intrusion in Iceland, *J. Volcanol. Geotherm. Res.*, *310*, 242–252, doi:10.1016/j.jvolgeores.2015.12.002.
- Humphris, S. E., and G. Thompson (1978), Hydrothermal alteration of oceanic basalts by seawater, *Geochim. Cosmochim. Acta*, *42*, 107–125, doi:10.1016/0016-7037(78)90221-1.
- Kelley, D. F., and M. Barton (2008), Pressures of crystallization of Icelandic magmas, *J. Petrol.*, *49*, 465–492, doi:10.1093/petrology/egm089.
- Longpré, M. A., A. Klügel, A. Diehl, and J. Stix (2014), Mixing in mantle magma reservoirs prior to and during the 2011–2012 eruption at El Hierro, Canary Islands, *Geology*, *42*, 315–318, doi:10.1130/G35165.1.
- Macpherson, C. G., D. R. Hilton, J. M. Day, D. Lowry, and K. Grönvold (2005), High-³He/⁴He, depleted mantle and low- $\delta^{18}\text{O}$, recycled oceanic lithosphere in the source of central Iceland magmatism, *Earth Planet. Sci. Lett.*, *233*, 411–427, doi:10.1016/j.epsl.2005.02.037.
- Marsh, B. D. (2013), On some fundamentals of igneous petrology, *Contrib. Mineral. Petrol.*, *166*, 665–690, doi:10.1007/s00410-013-0892-3.
- Martí, J., A. Castro, C. Rodríguez, F. Costa, S. Carrasquilla, R. Pedreira, and X. Bolos (2013), Correlation of magma evolution and geophysical monitoring during the 2011–2012 El Hierro (Canary Islands) submarine eruption, *J. Petrol.*, *54*, 1349–1373, doi:10.1093/petrology/egt014.
- Mollo, S., P. Del Gaudio, G. Ventura, G. Iezzi, and P. Scarlato (2010), Dependence of clinopyroxene composition on cooling rate in basaltic magmas: Implications for thermobarometry, *Lithos*, *118*, 302–312, doi:10.1016/j.lithos.2010.05.006.
- Morimoto, N., J. Fabries, A. K. Ferguson, I. V. Ginzburg, M. Ross, F. A. Seifert, J. Zussman, K. Aoki, and G. Gottardi (1988), Nomenclature of pyroxenes, *Am. Mineral.*, *73*, 1123–1133, doi:10.1007/BF01226262.
- Neave, D. A., E. Passmore, J. Maclennan, G. Fitton, and T. Thordarson (2013), Crystal–melt relationships and the record of deep mixing and crystallization in the AD 1783 Laki eruption, Iceland, *J. Petrol.*, *54*, 1661–1690, doi:10.1093/petrology/egt027.
- Neave, D. A., J. Maclennan, T. Thordarson, and M. E. Hartley (2015), The evolution and storage of primitive melts in the Eastern Volcanic Zone of Iceland: The 10 ka Grímsvötn tephra series (i.e. the Saksunarvatn ash), *Contrib. Mineral. Petrol.*, *170*, 1–23, doi:10.1007/s00410-015-1170-3.
- Nichols, A. R. L., M. R. Carroll, and Á. Höskuldsson (2002), Is the Iceland hot spot also wet? Evidence from the water contents of undegassed submarine and subglacial pillow basalts, *Earth Planet. Sci. Lett.*, *202*, 77–87, doi:10.1016/S0012-821X(02)00758-6.
- Nimis, P. (1995), A clinopyroxene geobarometer for basaltic systems based on crystal-structure modelling, *Contrib. Mineral. Petrol.*, *121*, 115–125, doi:10.1007/s004100050093.
- Norton, D., and H. P. Taylor (1979), Quantitative simulation of the hydrothermal systems of crystallizing magmas on the basis of transport theory and oxygen isotope data: An analysis of the Skaergaard Intrusion, *J. Petrol.*, *20*, 421–486, doi:10.1093/petrology/20.3.42.
- O’Driscoll, B., C. T. E. Stevenson, and V. R. Troll (2008), Mineral lamination development in layered gabbros of the British Palaeogene Igneous Province: A combined anisotropy of magnetic susceptibility, quantitative textural and mineral chemistry study, *J. Petrol.*, *49*, 1187–1221, doi:10.1093/petrology/egn022.
- Paquet, F., O. Dauteuil, E. Hallot, and F. Moreau (2007), Tectonics and magma dynamics coupling in a dyke swarm of Iceland, *J. Struct. Geol.*, *29*, 1477–1493, doi:10.1016/j.jsg.2007.06.001.
- Prestvik, T., S. Goldberg, H. Karlsson, and K. Grönvold (2001), Anomalous strontium and lead isotope signatures in the off-rift Öraefajökull central volcano in south-east Iceland: Evidence for enriched endmember(s) of the Iceland mantle plume?, *Earth Planet. Sci. Lett.*, *190*, 211–220, doi:10.1016/S0012-821X(01)00390-9.
- Putirka, K. D. (2005), Igneous thermometers and barometers based on plagioclase + liquid equilibria: Tests of some existing models and new calibrations, *Am. Mineral.*, *90*, 336–346, doi:10.2138/am.2005.1449.
- Putirka, K. D. (2008), Thermometers and barometers for volcanic systems, *Rev. Mineral. Geochem.*, *69*, 61–120, doi:10.2138/rmg.2008.69.3.
- Riel, B., P. Milillo, M. Simons, P. Lundgren, H. Kanamori, and S. Samsonov (2015), The collapse of Bárðarbunga caldera, Iceland, *Geophys. J. Int.*, *202*, 446–453, doi:10.1093/gji/ggv157.
- Sigmarsson, O., M. Condomines, K. Grönvold, and T. Thordarson (1991), Extreme magma homogeneity in the 1783–84 Lakagigar eruption: Origin of a large volume of evolved basalt in Iceland, *Geophys. Res. Lett.*, *18*, 2229–2232, doi:10.1029/91GL02328.
- Sigmarsson, O., I. Vlastelic, R. Andreasen, I. Bindeman, J.-L. Devidal, S. Moune, J. K. Keiding, G. Larsen, A. Höskuldsson, and T. Thordarson (2011), Remobilization of silicic intrusion by mafic magmas during the 2010 Eyjafjallajökull eruption, *Solid Earth*, *2*, 271–281, doi:10.5194/se-2-271-2011.
- Sigmundsson, F., et al. (2015), Segmented lateral dyke growth in a rifting event at Bárðarbunga volcanic system, Iceland, *Nature*, *517*, 191–195, doi:10.1038/nature14111.
- Sigurdsson, H., and S. R. J. Sparks (1978), Lateral magma flow within rifted Icelandic crust, *Nature*, *274*, 126–130, doi:10.1038/274126a0.

- Vennemann, T. W., and H. S. Smith (1990), The rate and temperature of reaction of ClF_3 with silicate minerals, and their relevance to oxygen isotope analysis, *Chem. Geol.*, *86*, 83–88, doi:10.1016/0168-9622(90)90008-Z.
- Winpenny, B., and J. Maclennan (2014), Short length scale oxygen isotope heterogeneity in the Icelandic mantle: Evidence from plagioclase compositional zones, *J. Petrol.*, *55*, 2537–2566, doi:10.1093/petrology/egu066.
- Yang, H. J., R. J. Kinzler, and T. L. Grove (1996), Experiments and models of anhydrous, basaltic olivine-plagioclase-augite saturated melts from 0.001 to 10 kbar, *Contrib. Mineral. Petrol.*, *124*, 1–18, doi:10.1007/s004100050169.
- Yoder, H. S., and C. E. Tilley (1962), Origin of basalt magmas: An experimental study of natural and synthetic rock systems, *J. Petrol.*, *3*, 342–532, doi:10.1093/petrology/3.3.342.